



# Modeling of Moving Table with Linear Roller Guides Subjected to Geometric Errors In Guide Rails

Van-Canh Tong<sup>1</sup> · Sun-Woong Kwon<sup>2</sup> · Seong-Wook Hong<sup>3</sup>

Received: 4 December 2019 / Revised: 16 July 2020 / Accepted: 22 July 2020 / Published online: 31 July 2020  
© Korean Society for Precision Engineering 2020

## Abstract

This paper presents a model of a linear roller guide that considers geometric errors in rails. A five degree-of-freedom model of a table supported by linear roller guides with guide rail errors was built to determine table-motion errors during its motion along erroneous rails. The model was verified by comparing the simulated displacements of a linear guide estimated by the proposed model and those by an existing transfer-function method. Two types of geometric errors were considered for the guide rail: general form and waviness errors. The influence of external load, initial preload, and a few important parameters of the rail—such as wavelength and amplitude—on the displacement of the carriage and table were investigated extensively. The simulation results demonstrated the ability of the model to obtain complicated motion errors for moving tables with a number of supporting linear guides subjected to guide errors.

**Keywords** Linear roller guide · Carriage · Linear table · Rail waviness error · Geometric error

## 1 Introduction

A linear guide unit consists of a guide rail and a carriage moving along the guide rail under rolling contact with balls or rollers. Linear guides are commonly employed in modern machine tools to support the movement of cutting tools or workpieces. Because the linear guide is directly responsible for the machine's axis movements, its precise motion plays a vital role in the precision of the whole machine [1,2]. However, unpredictable deviation in linear-guide dimensions from their ideal geometries is a common problem that causes deterioration of precision motion. Among them, straightness and angular errors are known to be two most common factors; these are often caused by the manufacturing process [3–5]. In addition, carelessness during the assembling

process can cause errors in linear-guide systems, for example, parallel misalignment in the rails and unequal height level of the rails. Moreover, during installation and use of the linear guide, various factors can produce relevant geometric imperfections such as unequal elastic deformation due to bolt fastening, unflattening of the mounting surface, and thermal distortion of the rail.

Studies on geometric errors and their influence on the motion accuracy of linear tables supported by linear bearings have attracted great attention from researchers. Rahmandi and Bleicher [6] examined the influence of geometric deviations on the performance of linear ball bearings in machine tools. Wang et al. [7] studied the statistical characteristics of the dynamics of linear ball bearings with random geometric parameters. The motion error of a table supported by multiple linear ball bearings with an erroneous guide rail has been analyzed using a transfer-function (TF) method [8–10]. Majda [11] simulated the joint kinematic errors of a machine tool caused by guideway geometric errors. He reported that geometric error of the guide rail is one of the major factors affecting the precision of machine tools. Zhang et al. [12] analyzed the guide-rail error in a hydrostatic bearing and showed that the motion error is related to the spatial frequency of the guide-rail error. Zhang et al. [13] estimated the motion error of a linear-bearing table considering guide-rail form errors. Later, they investigated the influences of

✉ Seong-Wook Hong  
swhong@kumoh.ac.kr

<sup>1</sup> Department of Ultra-Precision Machines and Systems, Korea Institute of Machinery and Materials, 156 Gajeongbuk-ro Yuseong-gu, Daejeon 34103, Republic of Korea

<sup>2</sup> Photomechanic Inc., 100, Inha-ro, Michuhol-gu, Incheon 22212, Republic of Korea

<sup>3</sup> Department of Mechanical System Engineering, Kumoh National Institute of Technology, 61 Daehak-ro, Gumi, Gyeongbuk 39177, Republic of Korea

geometrical errors of guideways on the positioning repeatability in the linear axes of machine tools [14]. The effect of geometric error in the linear guideway on the accuracy of a vertical three-axis CNC milling machine was investigated by Kwintarini et al. [15]. Fan et al. [16] predicted the kinematic errors of a multi-axis machine tool with guideways with dimensional tolerance. The aforementioned studies highlight that the geometric errors of guide rails have a significant influence on the motion errors of linear guideways, and the joint kinematic motion of the machine as a whole. Recently, Tong et al. [17] proposed a full analytical model to determine the stiffness matrix and displacement of a linear ball guide considering carriage flexibility.

Along with the analytical modeling approach, finite element (FE) analysis has also been used to analyze the motion error of linear-motion guides. Chlebus and Dybala [16] calculated the static properties of guideway joints based on an FE model. Kwon et al. [18,19] proposed a combined analytical and FE model to determine the static deflection of linear roller bearings. Majda [20] used the FE method to examine the relationship between kinematic straightness errors and angular errors of a table supported by guideways with geometric errors. He et al. [21] predicted the normal deformations of a guide rail and their effects on the joint kinematic errors of a horizontal machine center using FE analysis. Although the modeling method based on FE is advantageous over the analytical approach in terms of solving complicated systems, the FE approach is time-consuming.

To the authors' best knowledge, limited studies have focused on the geometric error of linear roller bearings. Most previous studies have analyzed linear ball bearings and relevant elements without any geometric imperfection. In reality, the geometric imperfection commonly occurs in mechanical joint elements such as rolling and linear bearings [22,23]. Because modeling of a linear roller bearing is very different from that of a linear ball bearing, existing models for ball bearings cannot be employed for roller bearings. Recently, several researchers have presented the motion error analysis results for linear roller guide and table system using the transfer function method [24,25]. However, the existing models commonly analyzed only two degree-of-freedom displacements for linear guide. This study proposes a general approach for the analysis of the effect of guide-rail error on the motion accuracy of a linear roller guide, as well as a table supported by multiple linear guides. The proposed method can determine five degree-of-freedom displacements of the table and linear roller guides simultaneously based on an effective use of vector and matrix method for reducing the complexity of the modeling and numerical procedure. The proposed model can be employed for a moving table with arbitrary number of linear guide sets under general external loading condition. This paper is structured as follows: In Sect. 2, we first present a description of the geometric error of the guide rail. Then, we describe how the

linear roller-guide model previously proposed by the authors [18] was modified to consider the geometric error of the guide rail. We constructed a new five degree-of-freedom model for a linear system with full components including a table and several linear roller guides. Section 3 presents the validation of the proposed model. We verified the proposed model by comparing the calculated displacements of the linear guide along an error rail with those determined by the TF method [8–10]. Subsequently, Sect. 4 presents the motion errors of the individual carriages, as well as a table with consideration of various error factors influencing the rail. Here, we considered two kinds of rail errors: a general form of rail error, and a fundamental waviness-form error described by a sinusoidal function. Finally, we provide conclusions in Sect. 5.

## 2 Modeling of Linear Roller Guide and Table

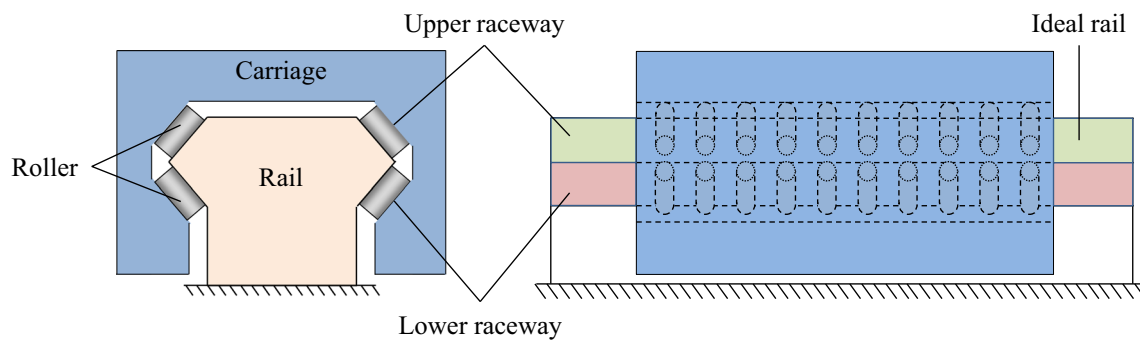
This section presents the model for the linear roller guide with rail error. The effect of accessories—such as the front and rear covers—and the roller retainer, are ignored because they have a negligible effect on the displacement of the carriage. A five degree-of-freedom table was constructed based on the model of the single linear roller guide.

### 2.1 Rail Error

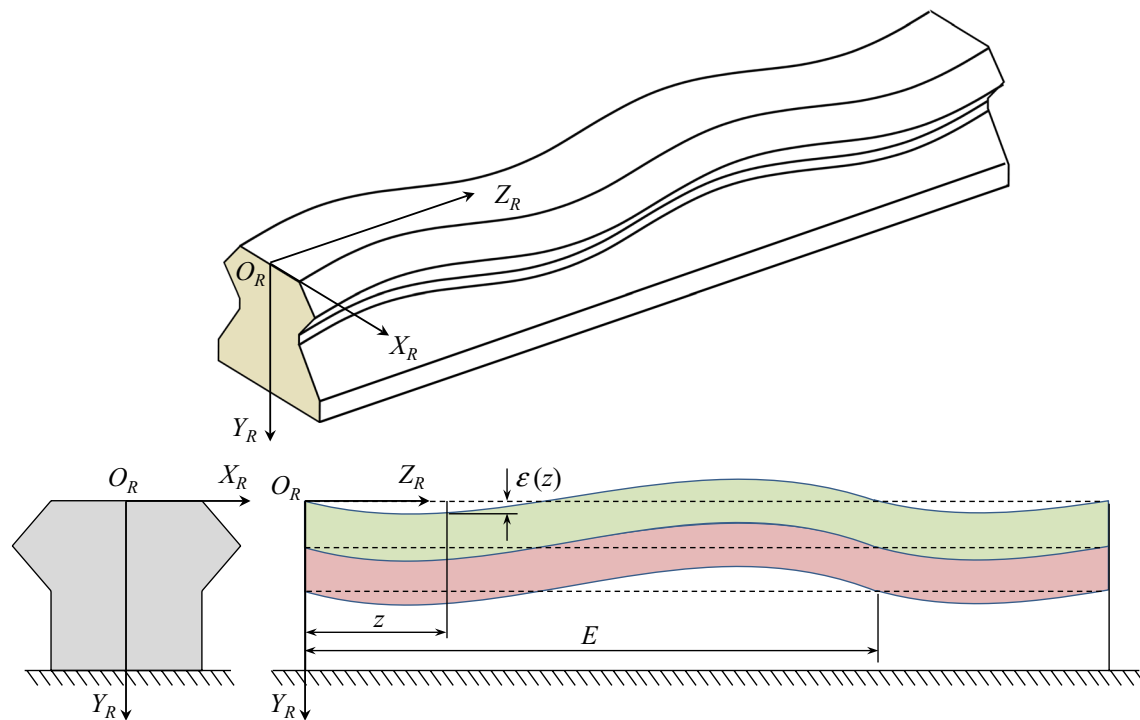
There are a number of possible geometric errors in a guide rail not only by its own geometric error but also by installation height or level mounting error, which may occur due to unflattening of the mounting surface, straightness errors, and rail misalignment. However, the purpose of this study is to develop and demonstrate a general analysis method for a moving table with multiple linear roller guides subjected to geometric errors in the guide rail. This study considers the rail geometric error in the vertical direction, as shown in Fig. 1b, for the purpose of showing the applicability of the proposed model. Figure 1 shows the linear roller guide with the ideal and error guides. To define the rail error, a coordinate system  $O_R X_R Y_R Z_R$  is used, in which origin point  $O_R$  is fixed at the left-end of the rail's upper surface. The error magnitude is mathematically represented by function  $\varepsilon(z)$ , as shown in Fig. 1. In general,  $\varepsilon(z)$  can bear any mathematical form. One fundamental form considered in this study is the sinusoidal (or waviness) error with the error magnitude at an axial distance  $z$  defined by:

$$\varepsilon(z) = \varepsilon_0 \sin\left(2\pi \frac{z}{E} + \phi\right) \quad (1)$$

where  $\varepsilon_0$  and  $E$  represent the error amplitude and wavelength of the error, respectively. Angle  $\phi$  is the phase angle.



(a) Linear roller guide with ideal rail



(b) Guide rail with error in plane  $O_R Y_R Z_R$

Fig. 1 Guide-rail error of linear roller bearing

### 2.2 Equilibrium of Carriage with Rail Error

The carriage equilibrium with the rail error was constructed based on a five degree-of-freedom linear roller bearing model [18]. The original model [18] was modified in this study to take into account the rail error. Figure 2 shows the linear roller bearing under external loads  $\{F\} = \{F_x, F_y, M_x, M_y, M_z\}^T$ , which causes displacements  $\{\delta\} = \{\delta_x, \delta_y, \gamma_x, \gamma_y, \gamma_z\}^T$ . These loads and displacements are defined based on a global coordinate system  $Oxyz$  with the origin located at the center point of the upper surface of the carriage (Fig. 2a). The position of the carriage on the rail is indicated by  $Z_O$ .

Figure 2b shows a cross-section of the linear roller guide determined at an axial distance  $l_j$ . Under external loading, the carriage and rollers are displaced from their original positions, whereas the rail is assumed to be fixed in the space. Accordingly, the displacements of the roller and carriage cross-section at the roller are indicated by  $\{u_i\} = \{u_{\xi i}, \theta_i\}^T$  and  $\{v_i\} = \{v_{\xi i}, \psi_i\}^T$ , ( $i = 1, \dots, 4$ ), respectively, as shown in Fig. 3a. In this figure,  $u_{\xi}$  and  $v_{\xi}$  are the displacements of carriage cross-section and roller along the axis that is normal to the roller centerline.  $\theta$  and  $\psi$  represent the titled angles of carriage cross-section and roller, respectively.  $i$  and  $j$  are the row and roller indexes, respectively.

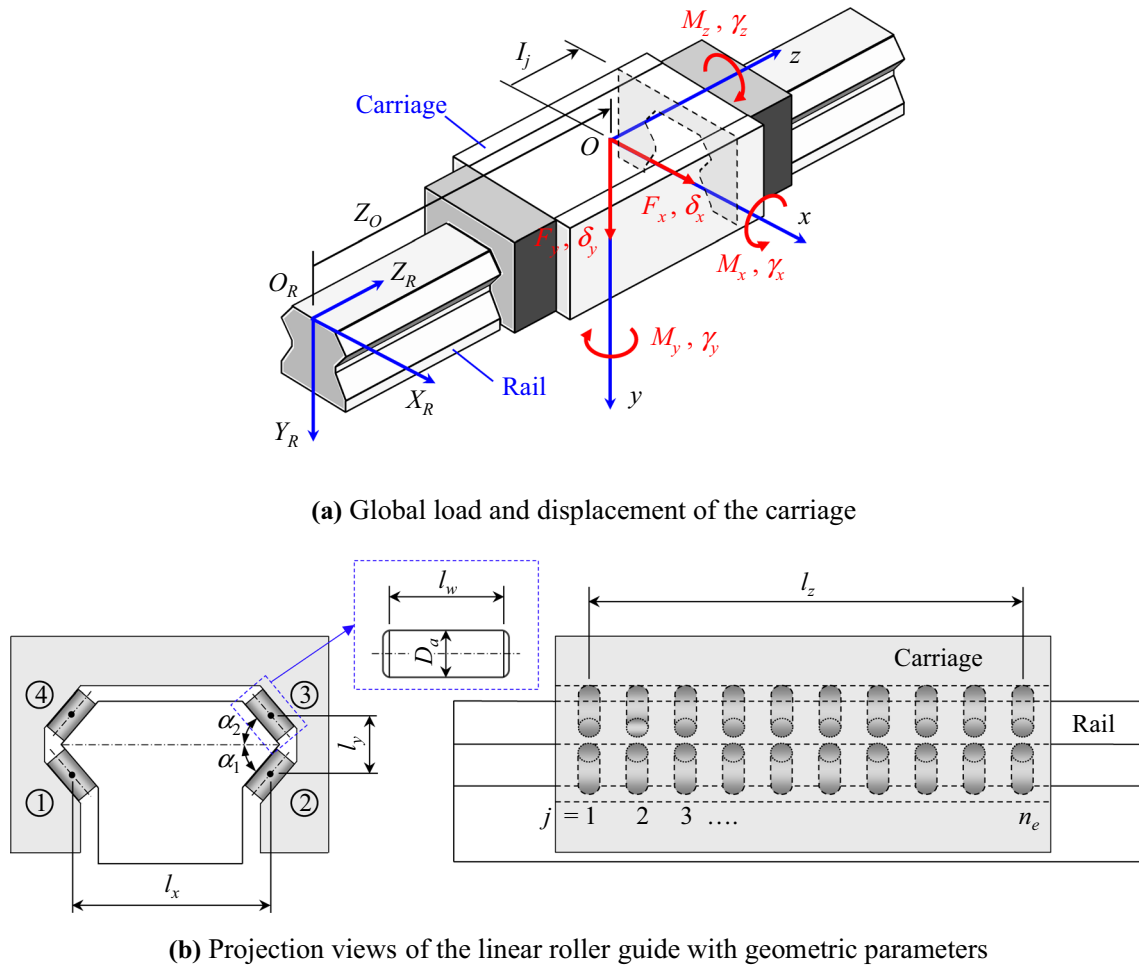


Fig. 2 Five degree-of-freedom model of the linear roller guide

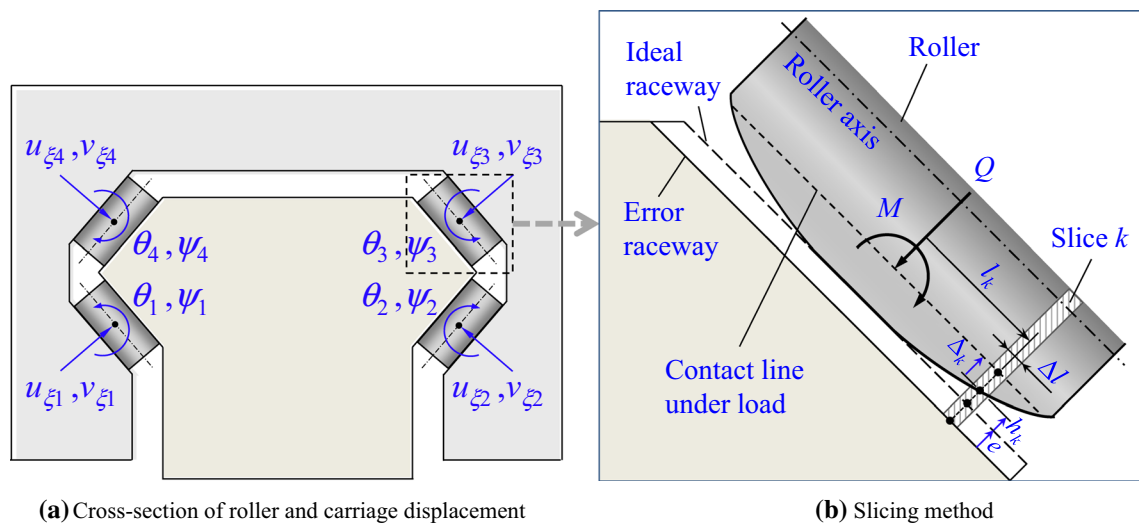


Fig. 3 Cross-section of roller and carriage displacements, which generates the contact load

Owing to the displacement of the rollers and carriage, the contact load— such as contact force  $Q$  and moment  $M$ —are generated at the contact point of the roller and raceways, which can be determined by the slicing method as illustrated in Fig. 3b:

$$Q = \sum_{k=1}^{n_s} q_k \tag{2}$$

$$M = \sum_{k=1}^{n_s} m_k \tag{3}$$

where the contact loads caused by a slice are equal to

$$q_k = c\Delta_k^{10/9} \Delta l, (\Delta_k > 0) \tag{4}$$

$$m_k = q_k l_k \tag{5}$$

where  $c$ ,  $\Delta l$ , and  $l_k$  represent the contact constant, contact length of the slice, and axial position of the  $k$ -th slice, respectively; and  $n_s$  is the total number of slices.  $q_k$  represents the contact force of a slice. The contact compression between the roller and the rail is calculated taking the rail error into account by:

$$\Delta_k = v_\xi + \psi l_k + \Delta_0 - h_k + e \tag{6}$$

where  $\Delta_0$  indicates the initial preload, which is equal to the amount of oversize of the roller diameter;  $h_k$  is the contact drop caused by the profiled roller; and  $e$  is the compression

caused by the rail error, which is determined for the rollers in rows 1 and 2 by:

$$e = \epsilon \cos \alpha_2 \tag{7}$$

and for the rollers in rows 3 and 4 by:

$$e = -\epsilon \cos \alpha_1 \tag{8}$$

The contact compression between the roller and carriage is calculated as:

$$\Delta_k = (u_\xi - v_\xi) + (\theta - \psi)l_k + \Delta_0 - h_k \tag{9}$$

The roller equilibrium equations can be generated from the roller and raceway contact loads, which are then solved to determine the roller displacements. Following this, the carriage equilibrium equation is built and then solved to determine the global displacement of the carriage. Details of the roller and carriage equilibrium equations are described in Ref.[18].

### 2.3 Equilibrium of Table Supported by Linear Guides with Rail Error

Figure 4 shows a table supported by four linear roller guides. A five degree-of-freedom model for the table is constructed. The table is loaded by an external load vector  $\{P\} = \{P_x, P_y, T_x, T_y, T_z\}^T$ , which causes displacements of  $\{\Delta\} = \{\Delta_x, \Delta_y, \Phi_x, \Phi_y, \Phi_z\}^T$ . The table is assumed rigid, and therefore the displacements of the table under load are only attributed to the displacements of the supporting linear roller guides. The

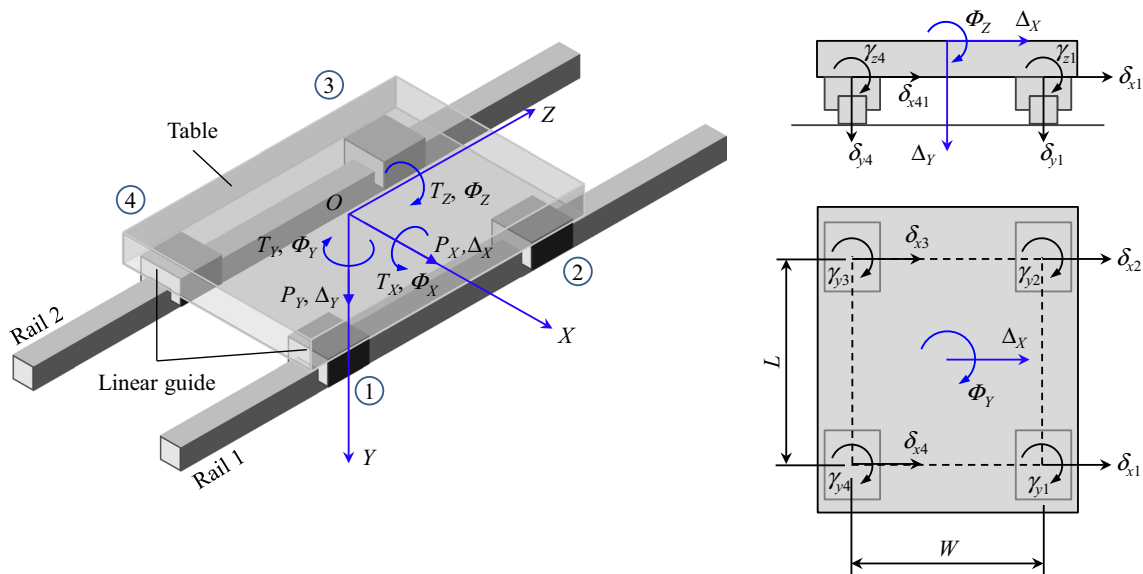


Fig. 4 Table supported by linear roller guides. Coordinate system  $OXYZ$  is introduced to determine displacement of the table, where  $O$  is located at the center of the table

displacements at each linear roller guide are related to the global displacements of the table as follows:

$$\delta_{x1} = \Delta_X - R\Phi_Y \cos\beta \tag{10}$$

$$\delta_{y1} = \Delta_Y + \frac{L}{2}\Phi_X + \frac{W}{2}\Phi_Z \tag{11}$$

$$\gamma_{x1} = \Phi_X \tag{12}$$

$$\gamma_{y1} = \Phi_Y \tag{13}$$

$$\gamma_{z1} = \Phi_Z \tag{14}$$

where  $R$  and  $\beta$  are calculated by:

$$R = \frac{1}{2}\sqrt{L^2 + W^2} \tag{15}$$

$$\beta = \tan^{-1}\left(\frac{W}{L}\right) \tag{16}$$

where  $L$  is the distance between the centers of two carriages on a guide rail.  $W$  is the distance between the centers of two guide rails. In a matrix form, these equations can be rewritten as:

$$\begin{Bmatrix} \delta_{x1} \\ \delta_{y1} \\ \gamma_{x1} \\ \gamma_{y1} \\ \gamma_{z1} \end{Bmatrix} = \begin{bmatrix} 1 & 0 & 0 & -R \cos \beta & 0 \\ 0 & 1 & L/2 & 0 & W/2 \\ 0 & 0 & 1 & 0 & 0 \\ 0 & 0 & 0 & 1 & 0 \\ 0 & 0 & 0 & 0 & 1 \end{bmatrix} \begin{Bmatrix} \Delta_X \\ \Delta_Y \\ \Phi_X \\ \Phi_Y \\ \Phi_Z \end{Bmatrix} \tag{17}$$

$$\text{or } \{\delta\}_1 = [K]_1 \{\Delta\} \tag{18}$$

where  $[K]$  represents the transformation matrix. Similarly, for carriages 2, 3, and 4, the relationship between the displacement vectors of the carriages and the table is written in the following form:

$$\{\delta\}_m = [K]_m \{\Delta\}, \quad (m = 1, \dots, 4) \tag{19}$$

where the remaining transformation matrices are given by:

$$[K]_m = \begin{cases} \begin{bmatrix} 1 & 0 & 0 & R \cos \beta & 0 \\ 0 & 1 & -L/2 & 0 & W/2 \\ 0 & 0 & 1 & 0 & 0 \\ 0 & 0 & 0 & 1 & 0 \\ 0 & 0 & 0 & 0 & 1 \end{bmatrix}, & m = 2 \\ \begin{bmatrix} 1 & 0 & 0 & -R \cos \beta & 0 \\ 0 & 1 & -L/2 & 0 & -W/2 \\ 0 & 0 & 1 & 0 & 0 \\ 0 & 0 & 0 & 1 & 0 \\ 0 & 0 & 0 & 0 & 1 \end{bmatrix}, & m = 3 \\ \begin{bmatrix} 1 & 0 & 0 & -R \cos \beta & 0 \\ 0 & 1 & L/2 & 0 & -W/2 \\ 0 & 0 & 1 & 0 & 0 \\ 0 & 0 & 0 & 1 & 0 \\ 0 & 0 & 0 & 0 & 1 \end{bmatrix}, & m = 4 \end{cases} \tag{20}$$

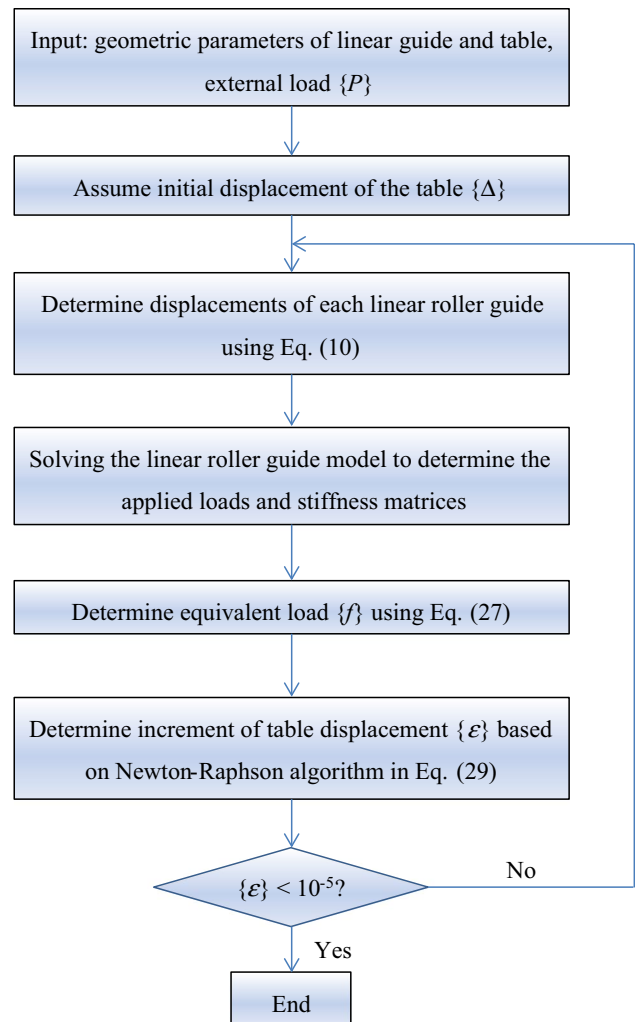
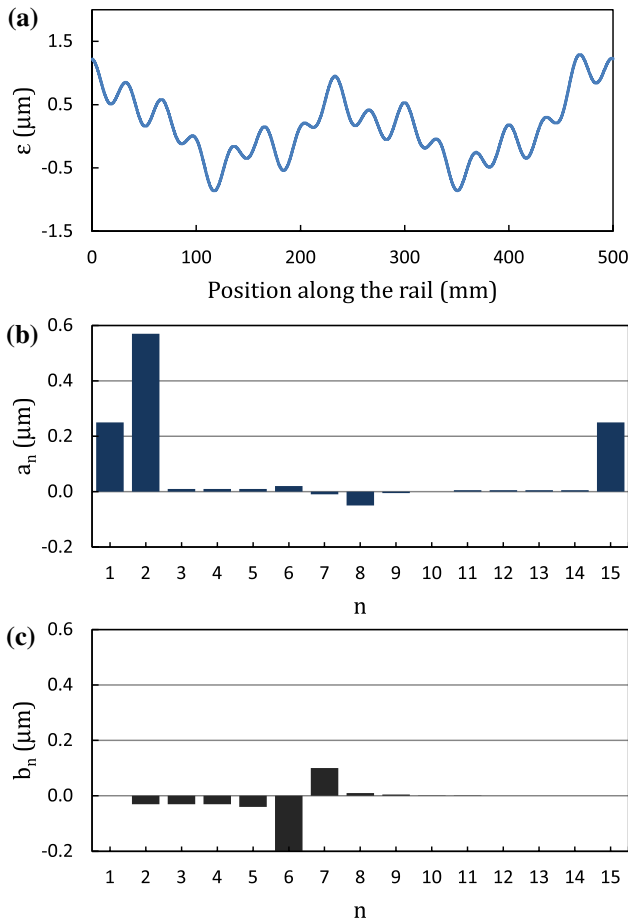


Fig. 5 Iterative scheme to solve the equilibrium of the table

**Table 1** Geometric parameters of linear roller guide and table

Parameter	Unit	Value	Parameter	Unit	Value
<i>Linear roller guide</i>					
Roller effective length $l_w$	mm	5.5	Lower contact angle $\alpha_1$	deg (°)	48
Horizontal distance of rows $l_x$	mm	29.76	Upper contact angle $\alpha_2$	deg (°)	48
Vertical distance of rows $l_y$	mm	8.58	Number of rollers per row $n_e$	–	24
Roller mean diameter $D_a$	mm	4.3	Carriage effective length $l_z$	mm	104
<i>Table</i>					
Longitudinal distance $L$	mm	400	Transversal distance $W$	mm	250



**Fig. 6** Assumed rail error, **a** shape of rail with error, **b** cosine coefficients, **c** sine coefficients

Knowing the displacements of a carriage, the applied load on the carriage  $\{F\}_m = \{F_{xm}, F_{ym}, M_{xm}, M_{ym}, M_{zm}\}^T$ , can be found using the linear guide model presented in the previous section, where  $m = 1, \dots, 4$  are the carriage index. However, with given displacements, the model equation can be solved without obtaining global equilibrium of the carriage; only the equilibrium of each roller is needed. The loads at the carriage are transformed to the global coordinate system of the table, resulting in equivalent loads; for carriage 1, these are:

$$f_{x1} = -F_{x1} \tag{21}$$

$$f_{y1} = -F_{y1} \tag{22}$$

$$m_{x1} = -\frac{L}{2}F_{y1} - M_{x1} \tag{23}$$

$$m_{y1} = R\cos\beta F_{x1} - M_{y1} \tag{24}$$

$$m_{z1} = -\frac{W}{2}F_{y1} - M_{z1} \tag{25}$$

or, in a matrix form:

$$\{f\}_1 = -[K]_1^T \{F\}_1 \tag{26}$$

The equivalent loads at the remaining carriages can be found in a similar manner. Then, the equivalent loads can be written in the following form:

$$\{f\}_m = -[K]_m^T \{F\}_m, \quad (m = 1, \dots, 4) \tag{27}$$

Summation of all equivalent loads  $\{f\}$  and external load  $\{P\}$  applied to the table yields the following equilibrium equations:

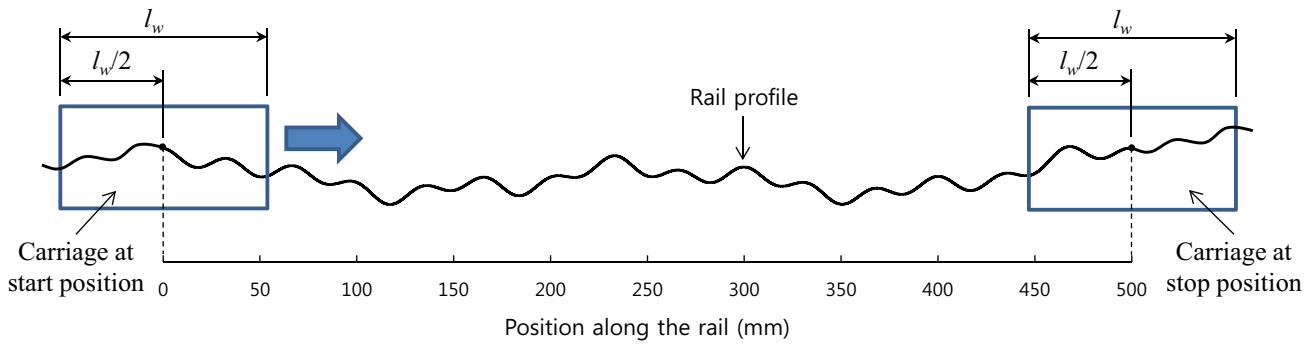
$$\{P\} + \sum_{m=1}^4 \{f\}_m = 0 \tag{28}$$

The iterative Newton–Raphson method is used to solve the table equilibrium equations. In the  $n$ -th loop of the iterative process, the algorithm of the Newton–Raphson method is written as

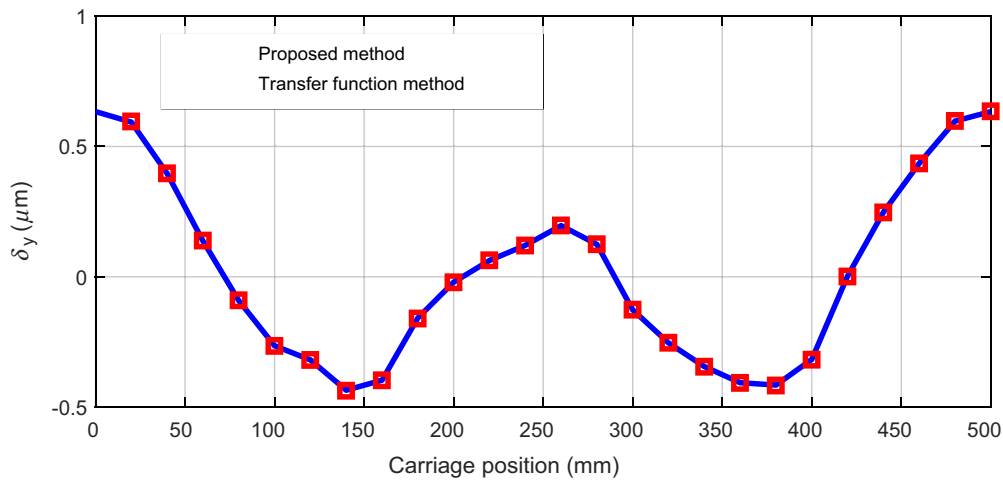
$$\{\varepsilon\} = -[J]^{-1} \left( \{P\} + \sum_{m=1}^4 \{f\}_m \right) \tag{29}$$

where  $\{\varepsilon\}$  is the increment of displacement vector  $\{\Delta\}$  of the table.  $[J]$  is a Jacobian matrix, determined by





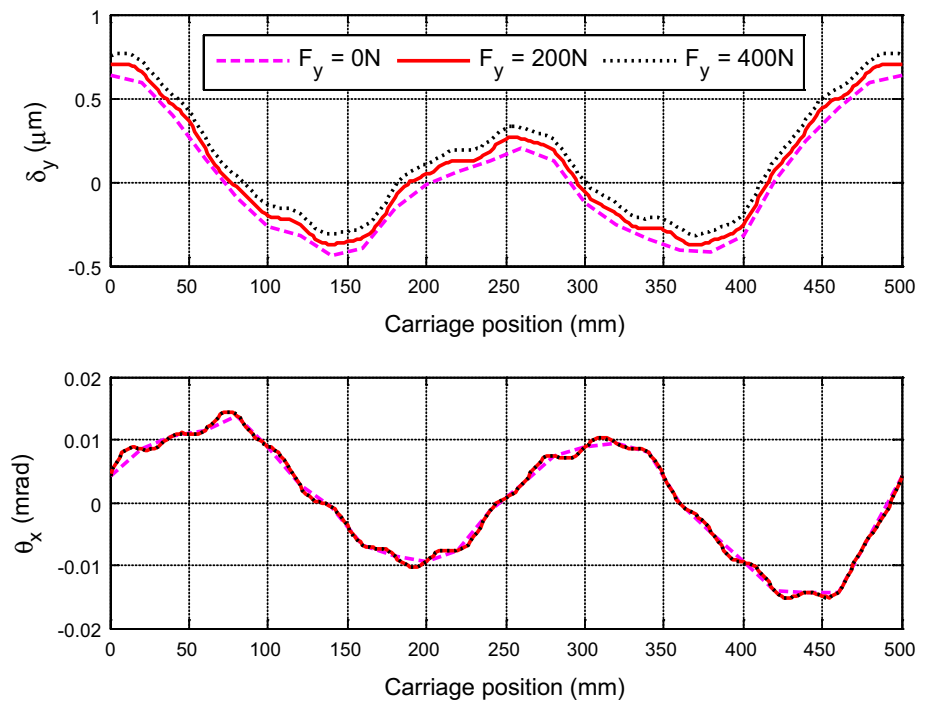
(a) Rail and linear guide carriage at start and stop positions



(b) Vertical displacement of carriage, estimated by the proposed method and TF method

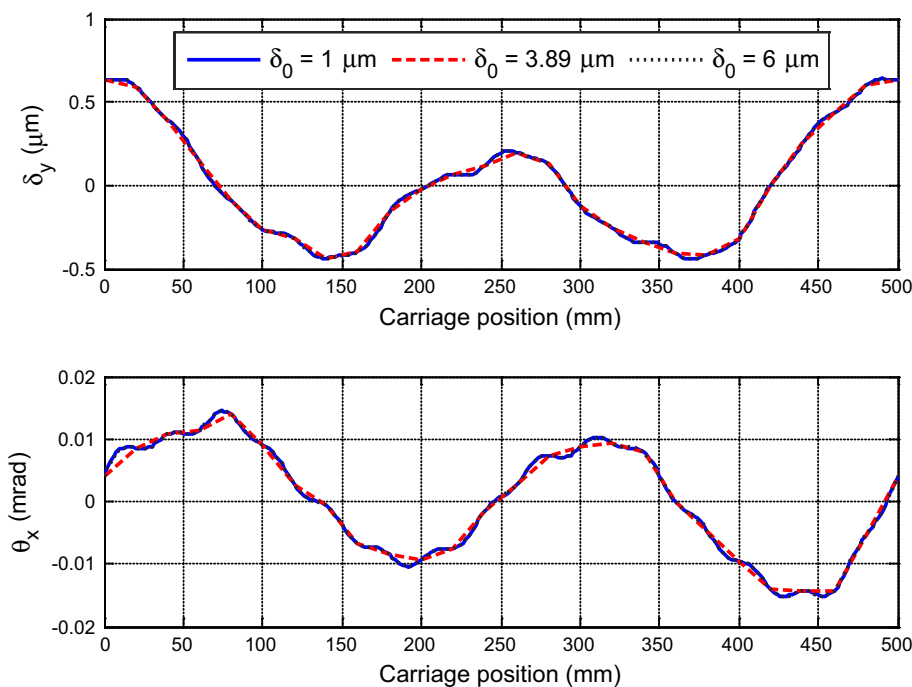
Fig. 7 Verification of single carriage displacement

Fig. 8 Effect of vertical load on displacement of carriage





**Fig. 9** Effect of preload on displacement of carriage (Fy=0 N)



$$[J] = \sum_{m=1}^4 [K]_m^T [F']_m [K]_m \tag{30}$$

where  $[F']$  represents the stiffness matrix of the linear guide, which is a  $(5 \times 5)$  matrix written as:

$$[F'] = \begin{bmatrix} \frac{\partial F_x}{\partial \delta_x} & \frac{\partial F_x}{\partial \delta_y} & \frac{\partial F_x}{\partial M_x} & \frac{\partial F_x}{\partial M_y} & \frac{\partial F_x}{\partial M_z} \\ \frac{\partial F_y}{\partial \delta_x} & \frac{\partial F_y}{\partial \delta_y} & \frac{\partial F_y}{\partial M_x} & \frac{\partial F_y}{\partial M_y} & \frac{\partial F_y}{\partial M_z} \\ \frac{\partial M_x}{\partial \delta_x} & \frac{\partial M_x}{\partial \delta_y} & \frac{\partial M_x}{\partial M_x} & \frac{\partial M_x}{\partial M_y} & \frac{\partial M_x}{\partial M_z} \\ \frac{\partial M_y}{\partial \delta_x} & \frac{\partial M_y}{\partial \delta_y} & \frac{\partial M_y}{\partial M_x} & \frac{\partial M_y}{\partial M_y} & \frac{\partial M_y}{\partial M_z} \\ \frac{\partial M_z}{\partial \delta_x} & \frac{\partial M_z}{\partial \delta_y} & \frac{\partial M_z}{\partial M_x} & \frac{\partial M_z}{\partial M_y} & \frac{\partial M_z}{\partial M_z} \end{bmatrix} \tag{31}$$

$[F']$  is calculated by:

$$[F'] = -[J_B] \tag{32}$$

where  $[J_B]$  represents the Jacobian matrix of the carriage global-equilibrium equations. Detailed calculations of  $[J_B]$  are presented in Appendix 1 of Ref.[18]. Figure 5 shows the computational process of the table equilibrium.

### 3 Simulation and Model Validation of Linear Roller Guide

This section presents the analysis of the characteristics of the table and linear roller bearing with rail error. The geometric parameters of the simulated linear roller guide and table are given in Table 1 and Fig. 2b.

#### 3.1 Model Verification

The displacement of the carriage along the error rail is calculated to verify the present model. The displacement results determined by the proposed model are compared with those calculated by a TF method, which has been clearly described and proved useful in several recent studies [7–9]. The TF method is applicable to general moving tables with multiple carriages, including single carriage. For more information of TF method, readers can refer to Refs.[8–10]. The linear guide is preloaded by a 3.89- $\mu\text{m}$  oversized roller diameter and is under no external loading. The rail error is represented by a Fourier series based on the wavelength of the guide-rail length as [8]:

$$\epsilon(z) = \sum_{n=1}^{15} \left[ a_n \cos\left(\frac{2n\pi}{E}z\right) + b_n \sin\left(\frac{2n\pi}{E}z\right) \right] \tag{33}$$

where  $E$  is the length of the guide rail;  $E = 500$  mm. Figure 6 plots the assumed guide-rail error and its Fourier coefficients from Eq. (33). Figure 7a displays the rail and

**Fig. 10** Vertical displacement of carriage with different rail-error periods ( $F_y=200$  N)

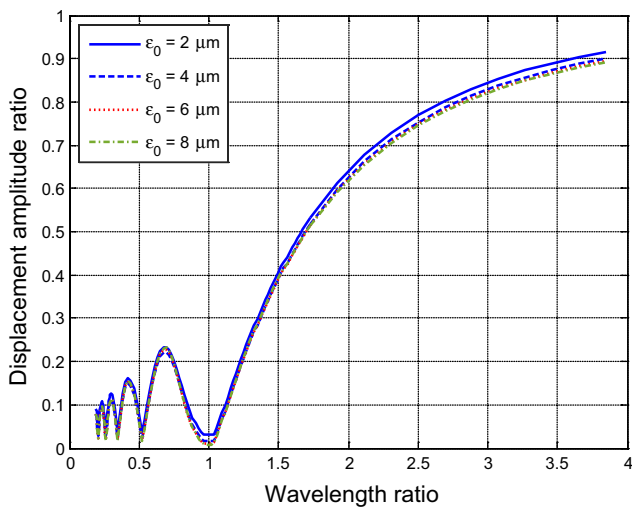
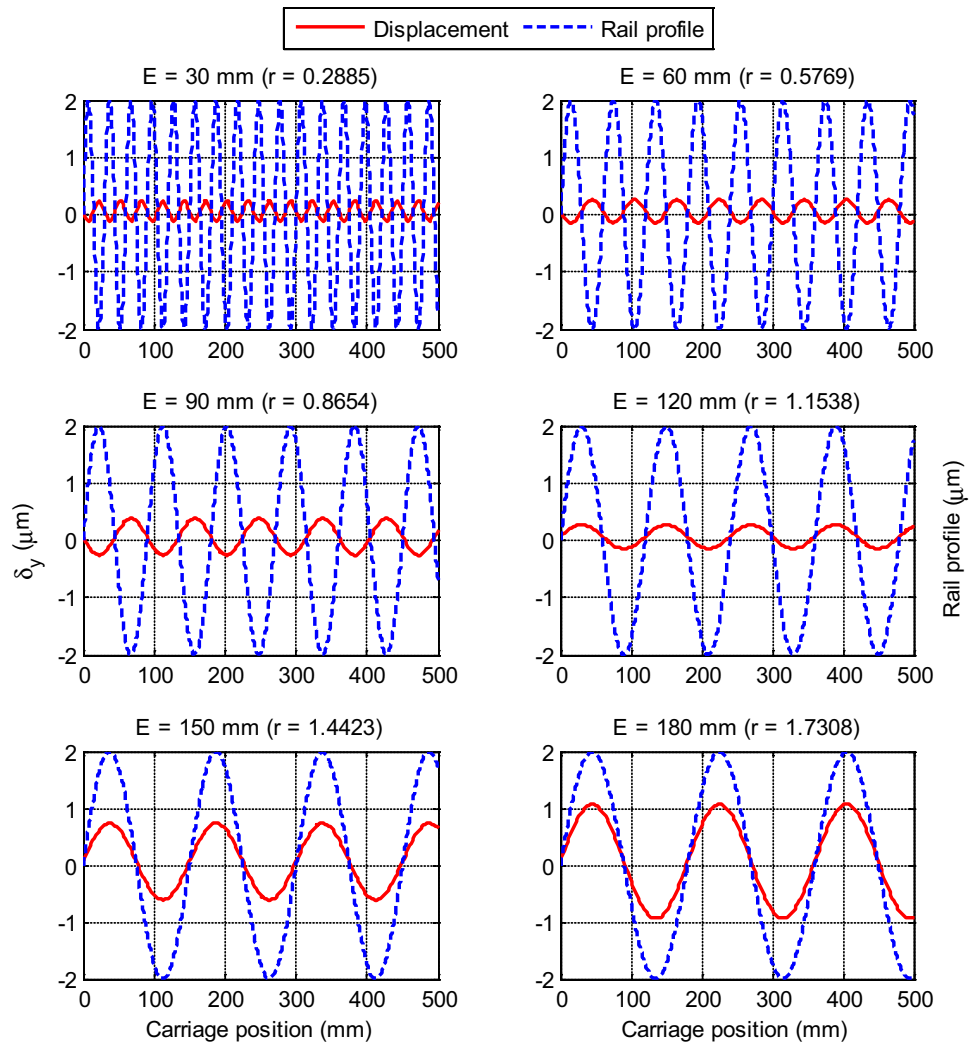


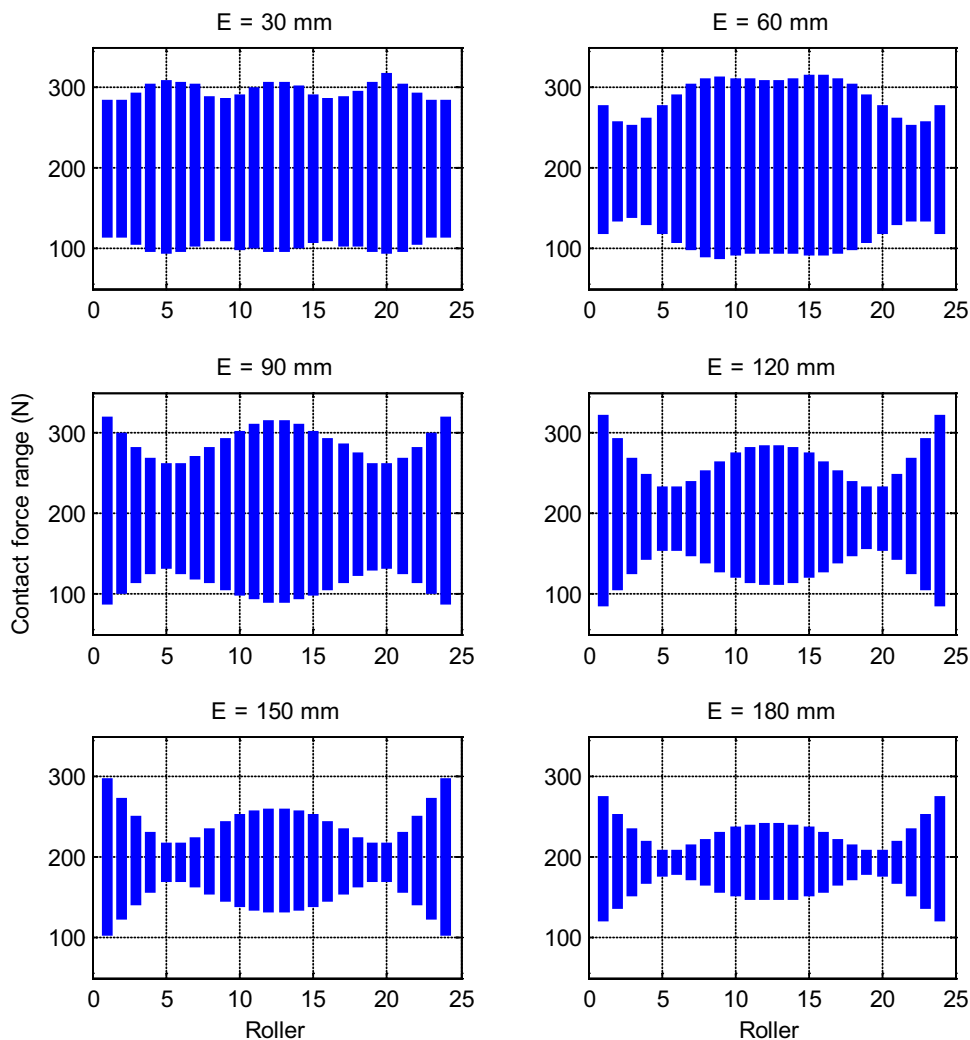
**Fig. 11** Vertical displacement amplitude of carriage with different error amplitudes ( $F_y=200$  N)

linear guide carriage at the start and stop positions. Figure 7b shows a comparison of the vertical displacement of the carriage calculated by the proposed model and the TF method. It is observed that the results of the two methods agree well with a negligible discrepancy.

### 3.2 Characteristics of Single Linear Roller Guide

This section details the investigation into the characteristics of the single linear roller guide, such as roller contact force and carriage displacement with rail error. First, consider the rail error as defined in Eq. (33). Figure 8 shows the effect of the vertical load on the displacement of the carriage. It is seen that a change in applied load leads to a parallel shift in the vertical-displacement curve with a slight change in its shape. This is explained by the fact that, when the applied vertical load increases, an identical contact force is added to all rollers in upper rows 3 and 4. Hence, the increments of contact compression caused by the added contact force are also similar for all rollers in rows 3 and 4, which leads to an identical

**Fig. 12** Contact-load range of rollers in row 1 with different wavelengths of rail error ( $F_y=200\text{ N}$ )



increment in the vertical displacement at different carriage positions. Further, Fig. 8 shows that the angular displacement of the carriage appears to be independent of loading condition.

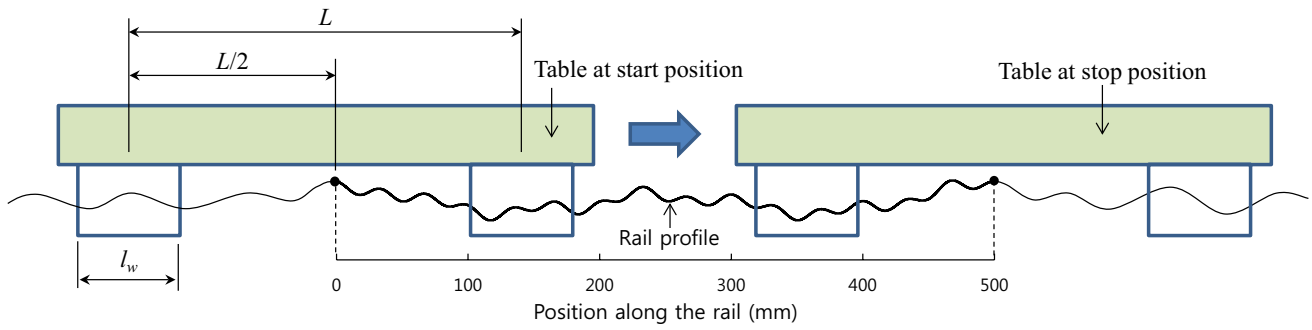
Figure 9 shows the effect of preload on the displacement of the linear guide with rail error. It is shown that the vertical displacement of the linear guide is not influenced by its preload. This is because the preload is adjusted by changing the diameter of all rollers. Then, if the preload is added, the same amount of additional compression is induced at all roller-raceway contacts, and therefore the contact forces of all rollers increase. As a result, the carriage remains balanced with increasing preload, without further displacement. Figure 9 also implies that the motion error of a linear roller guide caused by rail error may not be compensated by only changing its preload.

Next, consider a waviness rail error with the error function depicted in Eq. (1), which has an amplitude  $\epsilon_0$ , a fundamental period or wavelength  $E$ , and a phase angle  $\phi$ . Figure 10 shows the effect of wavelength  $E$  error on the displacement of the carriage. The error amplitude is selected as  $\epsilon_0 = 2\mu\text{m}$

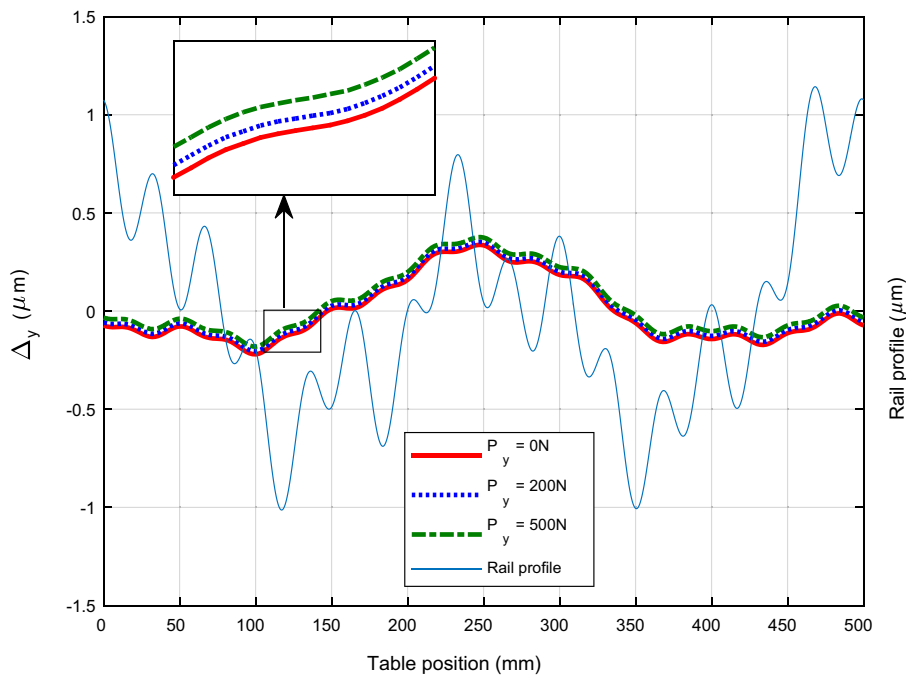
and the phase angle as  $\phi = 0$ . The displacement of the carriage becomes a sinusoidal curve with the same wavelength as the rail profile. The displacement and rail-profile curves can be in-phase or out-of-phase depending on the wavelength of the rail error. In general, if the wavelength ratio is less than 1.0, then  $180^\circ$  out-of-phase occurs. In contrast, the displacement and rail-profile curves are in-phase if the wavelength ratio is higher than 1.0. Here, the wavelength ratio ( $r$ ) is the ratio between the wavelength ( $E$ ) and effective length of the carriage ( $l_z$ ), as follows:

$$r = \frac{E}{l_z} \tag{34}$$

Figure 11 demonstrates the effect of the wavelength ratio  $r$  on the amplitude of the displacement of the carriage. This figure demonstrates the displacement-amplitude ratio, which is the ratio between the amplitude of the carriage displacement ( $\epsilon_\delta$ ) and that of the rail error ( $\epsilon_0$ ), as shown in Eq. (35).



(a) Rail and table at start and stop positions



(b) Displacement of table with rail-error profile according to Eq. (33)

Fig. 13 Rail and table positions and the displacement of table

$$\rho = \frac{\epsilon_\delta}{\epsilon_0} \tag{35}$$

It is observed that when the wavelength ratio is smaller than 1.0, there exists several values of  $r$  at which the displacement-amplitude ratio is minimized. However, when  $r$  exceeds 1.0, the displacement-amplitude ratio increases continuously. Moreover, the amplitude of rail error  $\epsilon_0$  has a negligible effect on the displacement-amplitude ratio, as shown in Fig. 11. Theoretically, when  $r$  is very large, the displacement of the carriage is very close to the rail profile and the displacement-amplitude ratio reaches 1.0.

Because of rail error, the contact force of the roller varies as the carriage moves along the rail. Figure 12 shows the range of contact force of the rollers in row 1, with

varying wavelength error. It is observed that the contact force is distributed over a larger range when the wavelength is small. The increasing wavelength of the rail error reduces the roller contact force, as well as the distributed range of contact force. Consequently, when the wavelength of the error is small, the rollers may experience severe loading conditions, which may have an adverse impact on the fatigue life of the linear roller guide.

### 4 Motion Characteristics Of Table

This section details the investigation into the effect of rail error on the motion characteristics of a table supported by four linear roller guides are investigated. All linear guide

**Fig. 14** Angular and lateral displacements of table in presence of rail-1 error

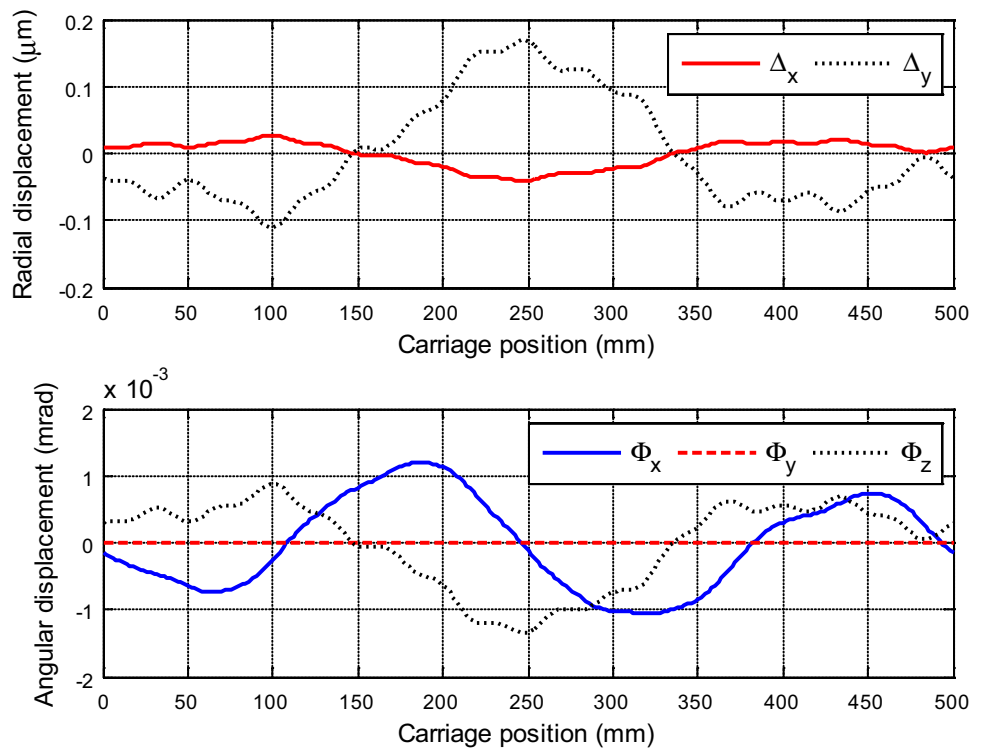
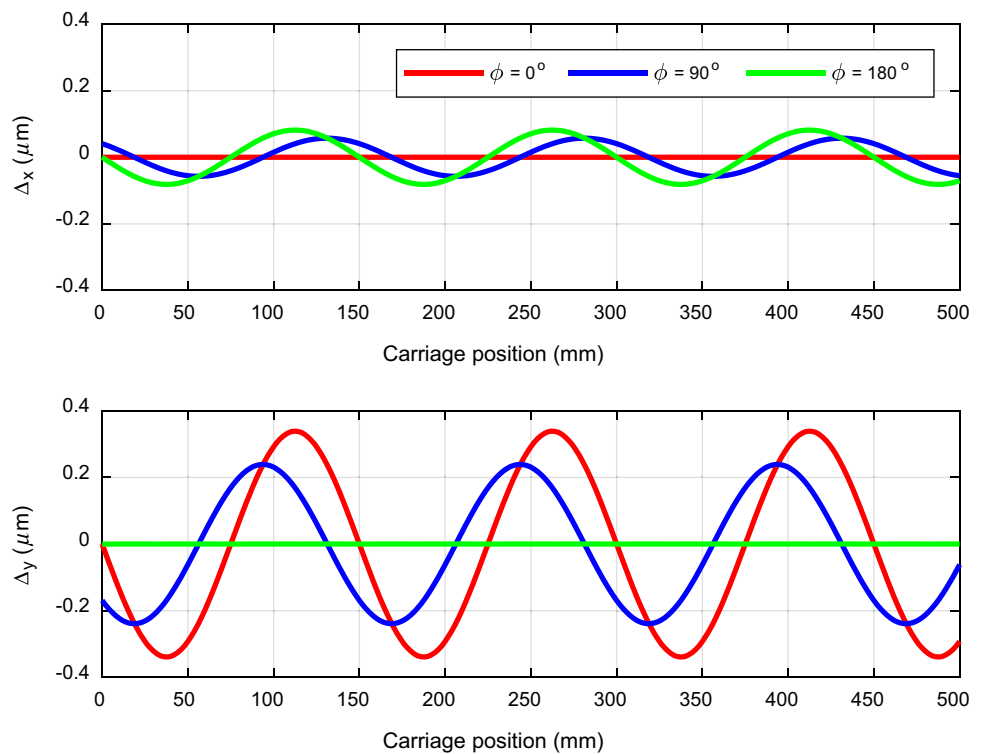


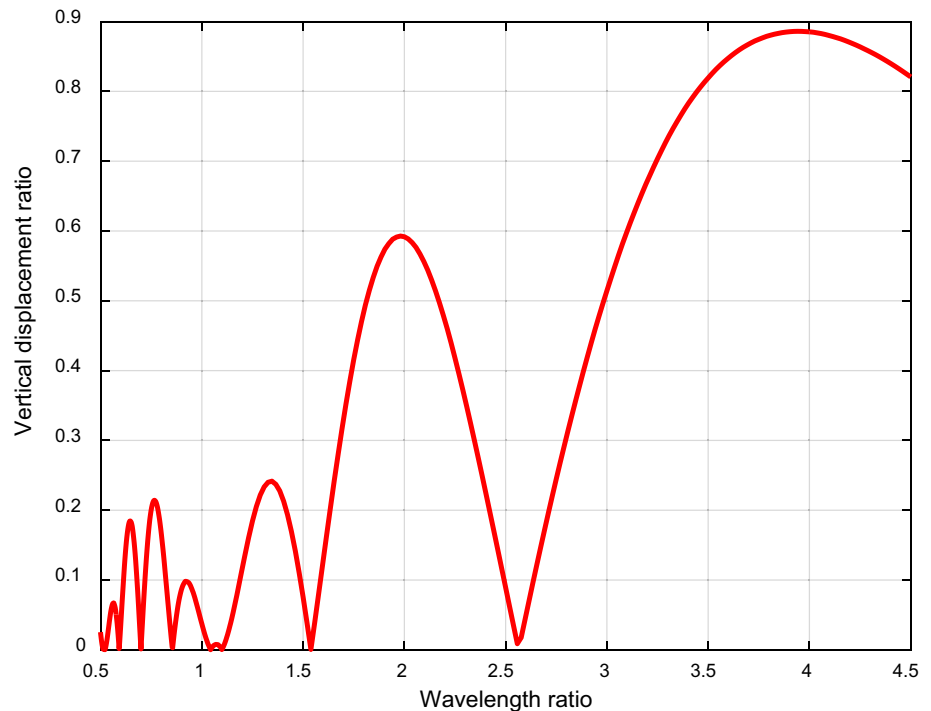
**Fig. 15** Effect of phase of rail 2 on displacement of table



blocks are preloaded by a 3.89- $\mu\text{m}$  oversized roller diameter. Figure 13a shows the rail and table at the start and stop positions. Figure 13b indicates the vertical displacement of the table subjected to increasing vertical load with two

rails with identical errors, as shown in Eq. (33). The moving distance of the table is set to  $S = 500$  mm. It is seen that the displacement amplitude of the table is smaller than that of the individual carriage moving on the same rail shown

**Fig. 16** Effect of wavelength ratio on vertical displacement of table



in Fig. 8. This is because the four carriage blocks are constrained by the rigid table. Because of restraint by the rigid table, the angular displacement components of all carriage blocks are equal, which could be attributed to the suppression of the vertical displacement. The increasing vertical load,  $P_y$ , acting at the table's center leads to a parallel shift in the displacement curves, which is similar to the behavior of the individual carriage shown in Fig. 8. Compared to the rail profile plotted in Fig. 13, it can be seen that the displacement of the table becomes smoother; this means that only low-frequency components of displacement are observed. It should be noted that the rail profile depicted in Fig. 13 represents the portion of the rail between the center of the table at the start and stop moving positions. To contain all linear blocks, the length of the whole rail is greater than moving distance  $S$ , because the table and linear block have their own length. The whole rail profile can be determined mathematically using Eq. (33).

To observe the remaining displacement components of the table, such as horizontal and angular displacements, only the rail-1 geometric error is considered, while rail 2 is assumed to be error free. Figure 14 shows all five displacement components of the table. As shown, the vertical displacement is dominant because rail error is assumed in the vertical plane (Fig. 1). The angular displacement  $\Phi_y$  is almost zero, while the two other components  $\Phi_x$  and  $\Phi_z$  have similar orders of magnitude.

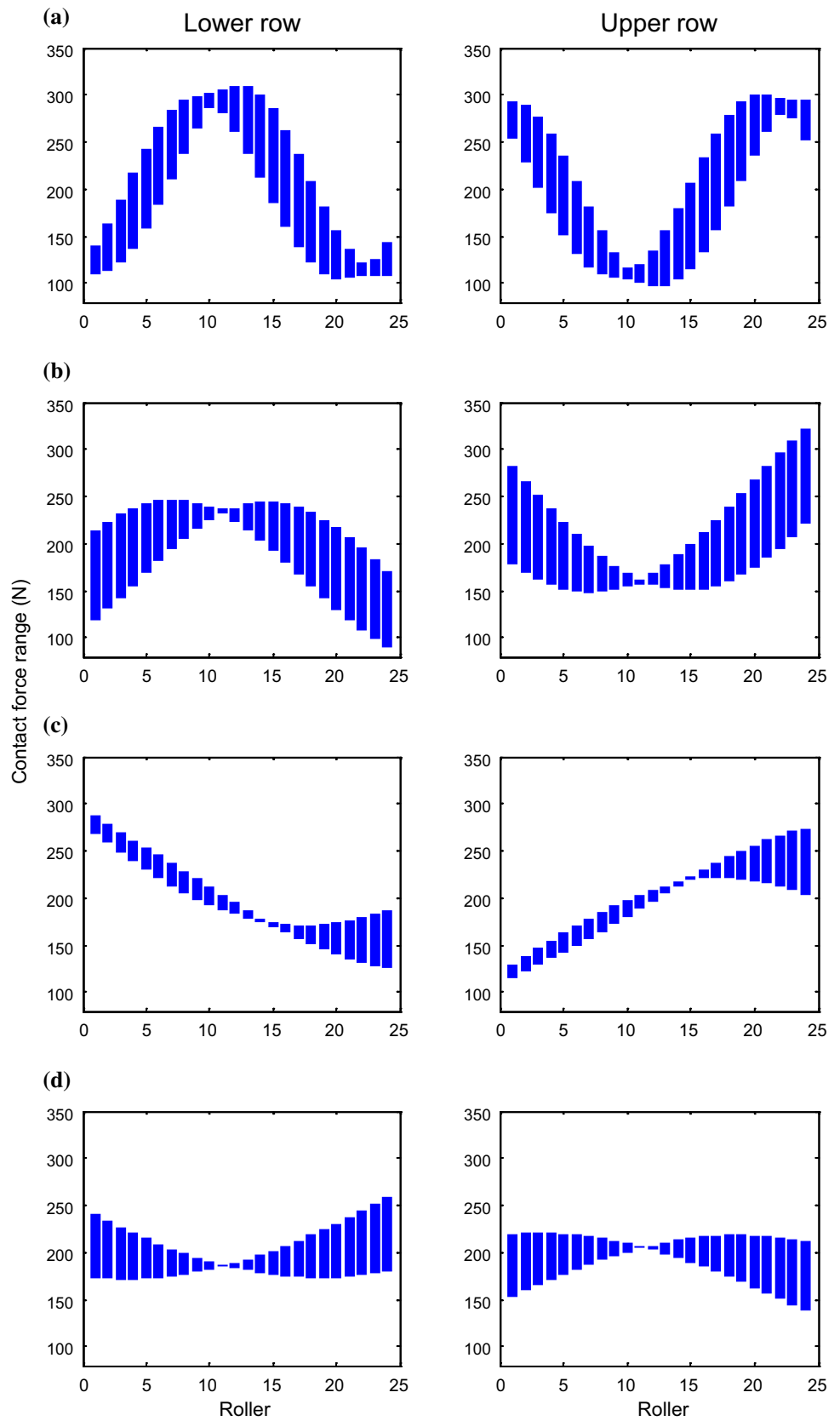
Next, consider a rail with waviness error as shown in Eq. (1). The effect of phase difference of two rails on the table displacement is considered. The phase angle of rail 1

is set to zero, whereas the phase angle of rail 2 is selected at  $0^\circ$ ,  $90^\circ$  and  $180^\circ$ . The amplitude and wavelength of the two rails are assumed identical. The amplitude is  $2 \mu\text{m}$  and the wavelength is  $150 \text{ mm}$ . Figure 15 shows the effect of phase difference on the displacement of the carriage. Horizontal displacement is induced, which is relatively small compared with vertical displacement. The vertical displacement of the table increases, whereas the horizontal displacement decreases with increasing phase difference.

Figure 16 shows the effect of wavelength ratio on the displacement-amplitude ratio of the table. The two rails are assumed to have identical waviness errors with a phase angle of zero and amplitude of  $2 \mu\text{m}$ . Only the vertical displacement is shown because it prevails over the other displacements. Unlike the displacement of a single linear guide block, the displacement curve of the table shows repeated parabolic segments throughout the wavelength ratio.

Figure 17 shows the variation in the contact-load range of the rollers determined for linear guide 1 with different wavelength ratios from one to four. It is seen that changing the wavelength ratio significantly changes the internal contact load of the rollers. In general, the contact loads of rollers become more uniform with increasing wavelength ratio. Moreover, the maximum contact loads of the rollers reduce with increasing wavelength ratio. The variation in contact force is reduced for the rollers at the middle of the carriage, whereas the rollers at the two ends suffer from higher load fluctuation. Hence, it can affect the performance characteristics such as carriage wear, heat generation, and fatigue life.

**Fig. 17** Contact-load range of rollers of linear-guide 1 with different wavelength ratios ( $r$ ), **a**  $r=1$ , **b**  $r=2$ , **c**  $r=3$ , **d**  $r=4$  ( $F_Y=0\text{ N}$ ,  $\phi=0^\circ$ )





## 5 Conclusions

In this study, a five degree-of-freedom model was proposed to determine the motion characteristics and roller contact forces of a table supported by several linear guides subjected to geometric errors. The proposed linear guide model was validated by means of comparison with the TF technique. The motion characteristics and contact loads of the linear guide and table were investigated for the cases of general-form error and fundamental-waviness error of the guide rails. The following conclusions are drawn from this study:

- Initial preload was unable to compensate the motion error of the linear guide and table with rail error.
- Increasing vertical load lead to a parallel shift in the displacement curves of both the linear guide and table.
- Although the rail contained high-frequency components, mainly low-frequency components were observed in the displacement of the carriage and table.
- When the wavelength ratio exceeded 1.0, the displacement amplitude of the single carriage moving on a rail with waviness error increased continuously. In this case, the displacement and rail profile curves were 180° out-of-phase with each other. When the wavelength ratio was below 1.0, the displacement curve of the carriage was in-phase with the sinusoidal rail profile. There were several wavelength ratios at which the displacement amplitude was minimized.
- The increasing wavelength of the rail error reduces the roller contact force, as well as the distributed range of contact force.
- When the wavelength of the error is small, the rollers may experience severe loading conditions, which may have an adverse impact on the fatigue life of the linear roller guide.
- As the wavelength ratio changed, the displacement amplitude of the table involved numerous parabolic segments over the entire wavelength-ratio range.

**Acknowledgements** This research was supported by National Research Foundation of Korea (Grant Number: NRF-2019R1F1A1063783).

## References

1. Okafor, A. C., & Ertekin, Y. M. (2000). Derivation of machine tool error models and error compensation procedure for three axes vertical machining center using rigid body kinematics. *International Journal of Machine Tools and Manufacture*, 40(8), 1199–1213.
2. Hung, J.-P., Lai, Y.-L., Lin, C.-Y., & Lo, T.-L. (2011). Modeling the machining stability of a vertical milling machine under the

influence of the preloaded linear guide. *International Journal of Machine Tools and Manufacture*, 51(9), 731–739.

3. Chen, Y.-T., Lin, W.-C., & Liu, C.-S. (2017). Design and experimental verification of novel six-degree-of freedom geometric error measurement system for linear stage. *Optics and Lasers in Engineering*, 92, 94–104.
4. Ohta, H., & Tanaka, K. (2010). Vertical stiffnesses of preloaded linear guideway type ball bearings incorporating the flexibility of the carriage and rail. *Journal of Tribology*, 132(1), 547–548.
5. Ma, J., Lu, D., & Zhao, W. (2016). Assembly errors analysis of linear axis of CNC machine tool considering component deformation. *The International Journal of Advanced Manufacturing Technology*, 86(1–4), 281–289.
6. Rahmani, M., & Bleicher, F. (2016). Experimental and numerical studies of the influence of geometric deviations in the performance of machine tools linear guides. *Procedia CIRP*, 41, 818–823.
7. Wang, W., Zhang, Y., & Li, C. (2017). Dynamic reliability analysis of linear guides in positioning precision. *Mechanism and Machine Theory*, 116, 451–464.
8. Khim, G., Park, C. H., Shamoto, E., & Kim, S. W. (2011). Prediction and compensation of motion accuracy in a linear motion bearing table. *Precision Engineering*, 35(3), 393–399.
9. Shamoto, E., Park, C. H., & Moriwaki, T. (2001). Analysis and improvement of motion accuracy of hydrostatic feed table. *CIRP Annals Manufacturing Technology*, 50(1), 285–290.
10. Khim, G., Oh, J. S., & Park, C. H. (2014). Analysis of 5-DOF motion errors influenced by the guide rails of an aerostatic linear motion stage. *International Journal of Precision Engineering and Manufacturing*, 15(2), 283–290.
11. Majda, P. (2012). Modeling of geometric errors of linear guideway and their influence on joint kinematic error in machine tools. *Precision Engineering*, 36(3), 369–378.
12. Zhang, P., Chen, Y., Zhang, C., Jun, Z., & Wang, T. (2018). Influence of geometric errors of guide rails and table on motion errors of hydrostatic guideways under quasi-static condition. *International Journal of Machine Tools and Manufacture*, 125, 55–67.
13. He, G., Sun, G., Zhang, H., Huang, C., & Zhang, D. (2017). Hierarchical error model to estimate motion error of linear motion bearing table. *The International Journal of Advanced Manufacturing Technology*, 93(5–8), 1915–1927.
14. Sun, G., He, G., Zhang, D., et al. (2018). Effects of geometrical errors of guideways on the repeatability of positioning of linear axes of machine tools. *The International Journal of Advanced Manufacturing Technology*, 98(9–12), 2319–2333.
15. Kwintarini, W., Wibowo, A., Arthaya, B., et al. (2018). Modeling of geometric error in linear guideway to improve the vertical three-axis CNC milling machine's accuracy. *IOP Conference Series: Materials Science and Engineering*, 319, 012015.
16. Chlebus, E., & Dybala, B. (1999). Modelling and calculation of properties of sliding guideways. *International Journal of Machine Tools and Manufacture*, 39(12), 1823–1839.
17. Tong, V. C., Khim, G., Hong, S. W., & Park, C. H. (2019). Construction and validation of a theoretical model of the stiffness matrix of a linear ball guide with consideration of carriage flexibility. *Mechanism and Machine Theory*, 140, 123–143.
18. Kwon, S. W., Tong, V. C., & Hong, S. W. (2016). Modeling of displacement of linear roller bearing subjected to external forces considering LM block deformation. *Transactions of the Korean Society of Mechanical Engineers A*, 40(12), 1077–1085.
19. Kwon, S. W., Tong, V. C., & Hong, S. W. (2019). Five-degree-of-freedom model for static analysis of linear roller bearing subjected to external loading. *Journal of Mechanical Engineering Science*, 233(8), 2920–2938.

20. Majda, P. (2012). Relation between kinematic straightness errors and angular errors of machine tool. *Advances in Manufacturing Science and Technology*, 36(1), 47–53.
21. He, G., Guo, L., Li, S., & Zhang, D. (2017). Simulation and analysis for accuracy predication and adjustment for machine tool assembly process. *Advances in Mechanical Engineering*, 9(11), 1–14.
22. Kwon, S. W. (2018). Modeling and application of linear roller bearing considering carriage deformation. Ph.D. thesis in Mechatronics, Kumoh National Institute of Technology (in Korean).
23. Tong, V. C., & Hong, S. W. (2017). Study on the stiffness and fatigue life of tapered roller bearings with roller diameter error. *Journal of Engineering Tribology*, 231(2), 176–188.
24. He, G., Sun, G., Zhang, H., et al. (2017). Hierarchical error model to estimate motion error of linear motion bearing table. *The International Journal of Advanced Manufacturing Technology*, 93, 1915–1927.
25. Ni, Y., Zhou, H., Shao, C., et al. (2019). Research on the error averaging effect in a rolling guide pair. *Chinese Journal of Mechanical Engineering*, 32, 72.

**Publisher's Note** Springer Nature remains neutral with regard to jurisdictional claims in published maps and institutional affiliations.



**Van-Canh Tong** is a Postdoc researcher in the Department of Ultra Precision Machines and Systems at Korea Institute of Machinery & Materials, Korea. His research interests are modeling and analysis of rolling and linear bearings.



**Sun-Woong Kwon** is a Senior researcher at Photomechanic Inc., Korea. His research interests are modeling and analysis of linear guides, and command shaping for positioning systems.



**Seong-Wook Hong** is a Professor in the Department of Mechanical System Engineering, Kumoh National Institute of Technology, Korea. His research interests include spindle and bearings modeling and analysis, command shaping for positioning systems, and structural vibration analysis and control for mechanical systems.